2026 IEEE International Symposium on Circuits and Systems (ISCAS) | 979-8-3315-7769-8/26/$31.00 ©2026 IEEE | DOI: 10.1109/ISCAS66217.2026.11562931

A 0.156 NEF Transimpedance Amplifier with Analog-Domain Multi-Band Fusion Technique for High-sensitivity and Broadband Hydrophones

Hongye Sheng, Jiao Xia, Yaohui Luan, Xinhang Xu, Zhiyuan Wu, Xili Wang, Yipeng Lu, Linxiao Shen
School of Integrated Circuits, Peking University, Beijing 100871, China

***Abstract*—Underwater acoustic systems employ bulky sonar devices with inherently limited bandwidth. This work addresses the fundamental sensitivity-bandwidth trade-off in piezoelectric micromachined ultrasonic transducer (PMUT) through an innovative analog-domain multi-band fusion technique. We present a multi-channel fused transimpedance amplifier (TIA) implemented in 180-nm CMOS for high-sensitivity, broadband hydrophones. The proposed architecture combines analog-domain signal fusion with a capacitive-feedback TIA topology, achieving simultaneous area and power efficiency. When integrated with a compact 3 mm × 2 mm PMUT array, the system demonstrates 129% fractional bandwidth and 523 V/MPa sensitivity. The single-channel configuration achieves an input-referred noise (IRN) density of 10 pA/$\sqrt{}$Hz@1MHz with noise efficiency factor (NEF) of 0.093 while the triple-channel design attains a NEF of 0.156, representing an exceptional low-power solution that enables high-resolution underwater sensing.**

***Index Terms*—Hydrophone, Ultrasound, Low noise amplifier (LNA), Bandwidth extension, Piezoelectric micromachined ultrasonic transducer (PMUT), fractional bandwidth, Noise efficiency factor (NEF).**

I. Introduction

Underwater acoustic systems have emerged as a critical technology for applications such as marine exploration [1], and acoustic communications [2], [3]. The hydrophone is the sensing front-end of an acoustic system, converting acoustic pressure waves into electrical signals. Recent advances in piezoelectric micromachined ultrasonic transducer (PMUT), benefiting from miniaturization and CMOS-compatible processes, provide a promising alternative to traditional bulky piezoelectric hydrophones with limited fractional bandwidth.

However, Fig. 1(a) shows the trade-off between bandwidth and sensitivity in PMUTs, which hinders the further application in the acoustic systems [4]. Since high-frequency ultrasound has high precision but shallow penetration, while low-frequency offers deep penetration but low precision, there is a need for a broadband and high-sensitivity ultrasound receiver [5].

To address this problem, Fig. 1(b) presents the proposed bandwidth extension in PMUTs, which combines fundamental and higher-order modes across different channels while maintaining high sensitivity to acoustic pressures. As shown in Fig. 1(c), a multi-channel PMUT array with different center

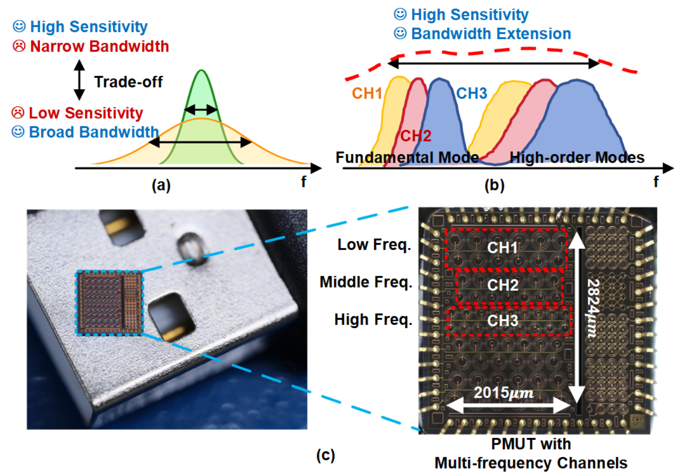

Fig. 1. (a) Trade-off between bandwidth and sensitivity in conventional PMUT; (b) The proposed PMUT bandwidth extension by combining fundamental mode and higher modes of different channels; (c) Optical image of broadband PMUT arrays with multi-channels to enhance the bandwidth of PMUTs.

frequencies is designed for this method of bandwidth extension. Direct parallel connection of multiple PMUTs offers a straightforward implementation, yet its sensitivity remains limited due to reactive energy coupling. Thus, a more promising approach involves separating PMUT channels and performing signal fusion at the ASIC level.

Single-band readout serves as the fundamental building block for multi-band systems, with extensive literature reporting implementations of ultrasonic readout chains [6]–[9]. To address impedance matching and low-noise challenges, the transimpedance amplifier is universally employed within the analog front-end (AFE), with implementations including resistive feedback (RF) [5], [10], [11] and capacitive feedback (CF) [8], [12]. Notably, despite the demonstrated advantages of multi-band architectures, existing solutions [6]–[9] predominantly focus on single-band designs, leaving a critical gap in multi-channel wide-bandwidth hydrophone readout AFEs.

To address this gap, this paper presents a triple-channel transimpedance amplifier using the analog-domain addition technique for the PMUT bandwidth extension and system-level optimization. The analog-domain strategy and the capacitive feedback TIA leads to a compact and power-efficient signal

This work was supported by the National Key Research and Development Program of China under Grant 2024YFB3212900. Corresponding author: Linxiao Shen (linxiao.shen@pku.edu.cn).

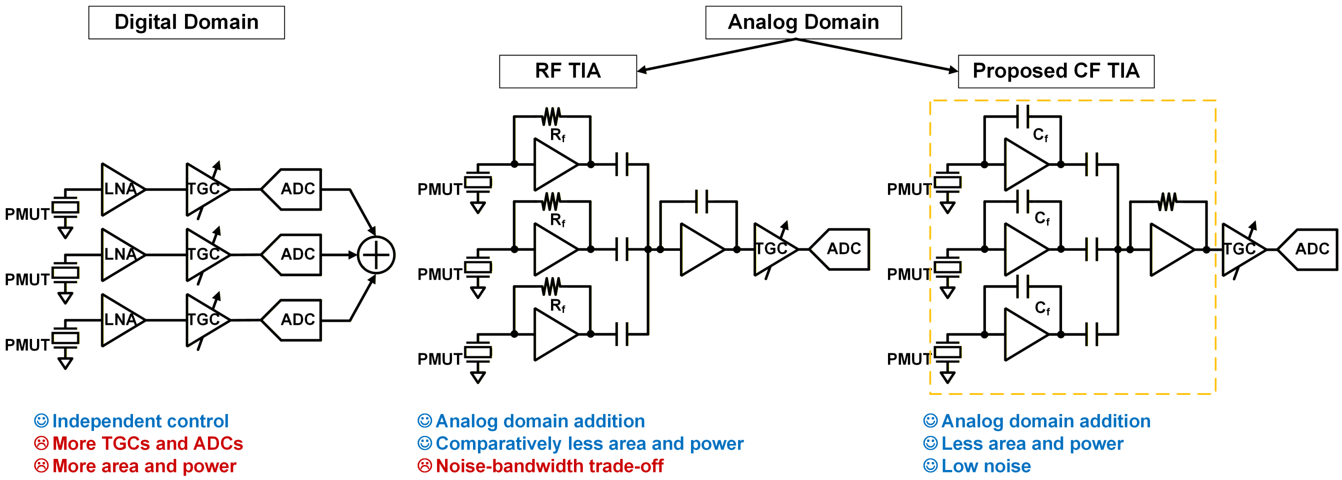

Fig. 2. Comparison between different structures of multi-channel addition for bandwidth extension.

chain with favorable noise performance, compared to its resistive counterparts. Furthermore, the designed differential circuit can ensure an inherent high power-supply rejection ratio without low dropout regulator [9] and can be naturally compatible to differential PMUT devices [13].

The organization of this paper is as follows: Section II outlines the imaging system and analyzes different structures. Section III describes the detailed circuit implementation of the designed amplifier. Section IV provides measurement results. And finally, Section V gives a conclusion for this work.

II. Imaging System and Structure Analysis

Fig. 2 shows the ultrasound receive (RX) signal chain of different structures to achieve multi-band fusion in ASIC and the electrical equivalent circuit model of the PMUT [14] is shown in Fig. 3. The conventional RX chain includes low noise amplifier (LNA), amplifier for time-gain compensation (TGC) and analog-to-digital converter (ADC). The purpose of TGC circuit is to compensate for signal attenuation with depth by providing a gain that increases with time.

The straightforward approach to implement the summation strategy is in the digital domain, as illustrated on the left side of Fig. 2. This method enables independent control over each channel. However, it requires additional TGC and ADC circuits, leading to increased area and power overhead. Moreover, this approach becomes incompatible with analog micro-beamforming (μBF), as the RX array scales in size and employs delay-and-sum operations [15]. Consequently, the analog-domain addition proves to be more power-saving and readily supports scaling to larger arrays.

The RF TIA structure is shown in the middle of Fig. 2. This architecture offers reduced area and power consumption; however, the inherent noise–bandwidth trade-off limits its applicability, especially for PMUTs with large C_P [7]. The input-referred current noise and bandwidth (BW) can be expressed

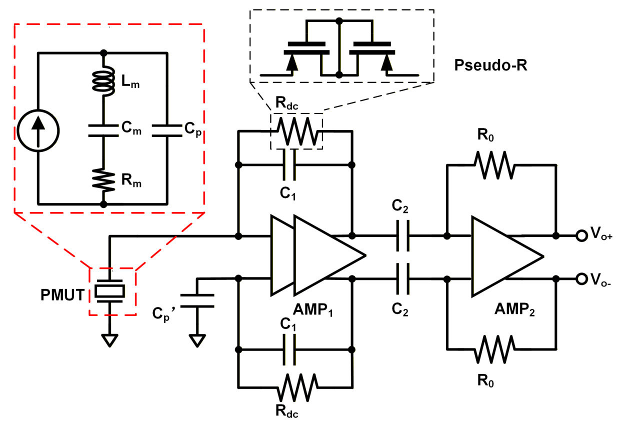

Fig. 3. Overall schematic of the proposed PMUT-ASIC system in the single-channel design.

as

$$i_{n,\mathrm{in}}^2 \approx \frac{4kT}{R_f} + V_{n,1}^2\left(\omega C_p + \frac{1}{R_f}\right)^2 \tag{1}$$

$$BW = \frac{1 + A_v}{R_f C_p} \tag{2}$$

where R_f is the feedback resistor, $V_{n,1}$ and A_v denote the input-referred noise and voltage gain of the first amplifier, respectively, C_p is the PMUT capacitance, k is Boltzmann's constant, and T is the absolute temperature. A larger R_f reduces noise but narrows bandwidth, whereas a smaller R_f increases bandwidth at the cost of higher noise, highlighting a fundamental trade-off between these two parameters.

Consequently, this paper chooses the structure of CF TIA to realize the multi-channel fusion technique, as shown on the right of Fig. 2. The analog architecture offers reduced area and power consumption relative to a digital solution. Furthermore, the capacitive feedback facilitates simultaneous low-noise and high-bandwidth performance. A detailed analysis of the proposed multi-channel CF TIA is presented in Section III.

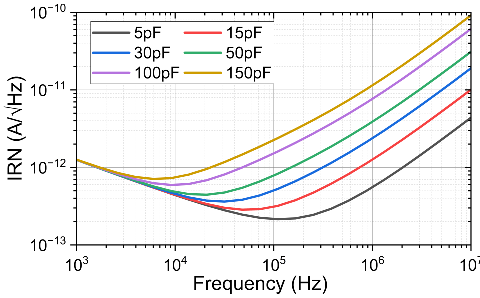

Fig. 4. Simulation results of input-referred noise of TIA with different PMUT capacitances.

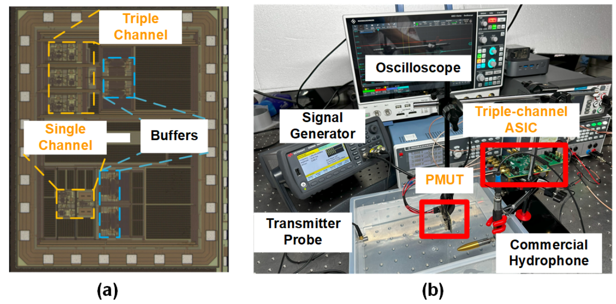

Fig. 5. (a) Chip micrograph of the single- and triple-channel LNA; (b) Test setup for the PMUT-ASIC system.

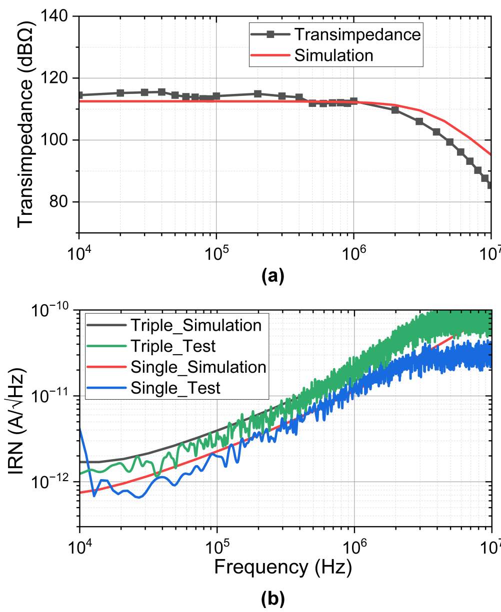

Fig. 6. (a) Measured transimpedance gain function of the proposed single-channel TIA; (b) Measured input-referred noise of the designed TIA.

III. Circuit Implementation

The designed circuit includes both single- and triple-channel ASIC implementations. A detailed circuit diagram of the single-channel version is provided in Fig. 3. The design will be comprehensively analyzed using the single-channel as a basis and then extended to the triple-channel configuration.

A. Closed loop configuration

Fig. 3 shows the PMUT-ASIC system in the single-channel configuration. At frequencies near the signal of interest, the analysis can be simplified by reducing the electrical equivalent circuit to a current source in parallel with a capacitor C_P, while temporarily neglecting the inductive-capacitive resonant branch. In the designed circuit, the transimpedance gain is set by $R_{total} = R_0 \times \frac{C_2}{C_1}$ and remains constant across the bandwidth.

In order to increase the bandwidth to satisfy the demand of PMUT's intrinsic center, the amplifier AMP_1 adopts a two-stage structure. The first stage employs a folded-cascode topology to ensure high open-loop gain, while the second stage is implemented with a basic fully differential common-source amplifier. Both stages utilize local common-mode feedback (CMFB) to stabilize their operating points. This structure gives the bandwidth as follows:

$$BW = \frac{C_1}{C_1 + C_p} \times \frac{g_{m1}}{C_{c,eq}} \tag{3}$$

where g_{m1} is the transconductance of the first-stage amplifier, $C_{c,eq}$ is the equivalent compensating capacitor. Consequently, the bandwidth can be widened by increasing I_d without degrading the noise performance, which is better than RF TIA.

B. Noise analysis

The noise is an important factor to be considered to optimize the system-level performance while designing the CF TIA. The input-referred noise of TIA can be calculated as

$$i^2_{n,in,Single} \approx V_n^2 \omega^2 (C_p + C_1)^2 \tag{4}$$

where V_n is the input-referred noise (IRN) of the two-stage amplifier. As shown in Fig. 4, the IRN has a peaking behaviour because the amplifier's voltage noise is converted to current noise by capacitor C_p. Meanwhile, it can be observed that the equivalent input-referred current noise exhibits a positive correlation with C_p. Consequently, in order to enable a more comprehensive comparison of the overall performance, the noise efficiency factor was introduced in [7]

$$\text{NEF} = \frac{i_{n,in} \cdot \sqrt{Power_{LNA}}}{C_{PMUT}} \tag{5}$$

where $i_{n,in}$ is the IRN noise, C_{PMUT} is the capacitance in the equivalent model, $Power_{LNA}$ is the power consumption of LNA.

C. Extension to Triple Channels

The triple-channel circuit is built upon the previously mentioned single-channel design. As shown on the right side of Fig. 2, the capacitor C_2 in Fig. 3 is split into three equal parts, while R_0 and feedback capacitor C_1 remains constant. Current signals from different channels are summed at the virtual ground of amplifier AMP_2 and share the same transimpedance gain, which is one-third that of the single-channel design. Since the noise power from different channels

TABLE I
PERFORMANCE SUMMARY AND COMPARISON WITH PRIOR WORKS.

	This work		**ISSCC'20 [8]**	**TBCAS'17 [11]**	**TBCAS'21 [5]**	**ASSCC'23 [7]**
Process [nm]	**180**		180	65	40	180
Transducer	**PMUT**		CMUT	CMUT	CMUT	CMUT
Center Frequency [MHz]	**Multi-frequency Fusion**		5	5	Tunable[a]	7.5
LNA Architecture	**CF TIA**		CF TIA	RF TIA	RF TIA	Current Conveyor
Bandwidth Extension	×	✓	N.A.	N.A.	N.A.	N.A.
Max LNA Gain [dBΩ]	**114**	**104**	106	97	90	106
Rx Power/Ch. [mW]	**1.94**	**1.8**	4.9	0.18	1.45	1.21
LNA Area/Ch. [mm^2]	**0.057**	**0.041**	0.12	0.0035	<0.025	0.045
Capacitance [pF]	**150**	**150**	15	5.5	25	25
IRN Density @Fc&Cp [pA/$\sqrt{}$Hz]	**10.0 @1MHz&150pF**	**17.5 @1MHz&150pF**	2.0 @5MHz&15pF	4.8 @5MHz&5.5pF	3.1 @3-18MHz&25pF	2.0 @7.5MHz&25pF
NEF[b] [pA/pF$\sqrt{}$(mW/Hz)]	**0.093**	**0.156**	0.3	0.37	0.15	0.088

[a] The capacitive micromachined ultrasonic transducer (CMUT) center frequency is tunable by DC bias voltage.
[b] NEF is defined in (5), which was introduced by [7].

also adds up at the output node, the IRN deteriorates by a factor of $\sqrt{3}$ compared to the single-channel design. In single-channel RX ASIC, CF TIA usually requires more area than RF TIA because of the capacitor, so the area-critical RX arrays may choose the RF TIA architecture at the expense of noise performance. However, the multi-channel application changes this condition, because capacitors are hard to eliminate in the precision adder design as shown in the middle of Fig. 2.

IV. MEASUREMENT RESULTS AND DISCUSSION

The amplifier is fabricated using a 180 nm CMOS process, including two designs of single-channel and triple-channel receivers. The chip micrograph and the test environment is shown in Fig. 5. Buffers are needed for the measurement. The section IV includes two parts, consisting of ASIC performance and PMUT-ASIC system performance.

A. ASIC performance

The measured transimpedance gain function in the single channel is shown in Fig. 6(a), achieving a gain of 114 dBΩ within the 10 kHz to 2 MHz range. Fig. 6(b) shows the input-referred noise results of simulation and measurement. The single-channel design achieves an IRN density of 10 pA/$\sqrt{}$Hz@1MHz at 1.94 mW, yielding a capacitor-normalized NEF of 0.093 according to (5). The triple-channel design still maintains a competitive NEF of 0.156, and meets the requirements for PMUT bandwidth extension.

B. PMUT-ASIC system performance

As presented in Fig. 7(a), the measured system sensitivity-frequency results consist of different channels and the triple-channel addition. While a single channel faces a sensitivity-bandwidth trade-off, in contrast, the triple-channel design achieves both a receiving sensitivity of 523 V/MPa and a 129% bandwidth, thereby validating the analog-domain bandwidth extension strategy. Fig. 7(b) plots the measured time-domain waveforms of the received ultrasonic waves across different frequencies, demonstrating the functionality of the PMUT-ASIC system.

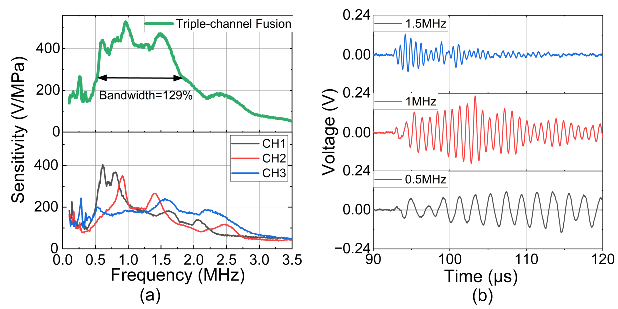

Fig. 7. (a) Measured sensitivity results of individual channels and the fused triple-channel design in the PMUT-ASIC system; (b) Time-domain waveforms at different signal frequencies.

Table I summarizes the performance comparison between the proposed ultrasound amplifier and prior works. Even under the largest capacitance C_P of 150 pF, the proposed CF TIA achieves competitive performance relative to existing designs, along with a favorable NEF normalized to the PMUT's C_P. Furthermore, the analog-domain fusion technique for PMUT bandwidth extension enables area and power savings in the RX signal chain.

V. CONCLUSION

In this paper, a multi-band fusion technique is proposed to overcome the fundamental sensitivity-bandwidth trade-off in PMUT-based underwater acoustic receivers. The multi-channel TIA combines analog-domain signal fusion with a capacitive-feedback topology. The integrated system with optimized PMUT achieves 129% fractional bandwidth and 523 V/MPa sensitivity. Meanwhile the receiver core in the single-channel configuration attains a 10 pA/$\sqrt{}$Hz IRN density and a 0.093 NEF with the triple-channel design attaining an NEF of 0.156. This circuit is a promising solution for broadband and high-sensitivity hydrophones in acoustic applications.

REFERENCES

[1] Z. Zhou, C. Liu, L. Jia, L. Shi, X. Wang, J. Tao, C. Sun, and G. Wu, "A ScAlN piezoelectric high-frequency acoustic pressure-gradient MEMS vector hydrophone with large bandwidth," *IEEE Electron Device Letters*, vol. 43, no. 7, pp. 1109–1112, 2022.

[2] B. Herrera, F. Pop, C. Cassella, and M. Rinaldi, "Miniaturized PMUT-based receiver for underwater acoustic networking," *Journal of Microelectromechanical Systems*, vol. 29, no. 5, pp. 832–838, 2020.

[3] M. Stojanovic and J. Preisig, "Underwater acoustic communication channels: Propagation models and statistical characterization," *IEEE Communications Magazine*, vol. 47, no. 1, pp. 84–89, 2009.

[4] Y. Zhang, T. Jin, Y. Deng, and et al., "A low-voltage-driven MEMS ultrasonic phased-array transducer for fast 3D volumetric imaging," *Microsystems & Nanoengineering*, vol. 10, p. 128, 2024.

[5] M. Zhou, S. Ouzounov, E. Cantatore, and P. Harpe, "An RX AFE with programmable BP filter and digitization for ultrasound harmonic imaging," *IEEE Transactions on Biomedical Circuits and Systems*, vol. 15, no. 6, pp. 1430–1440, 2021.

[6] M. Tan, C. Chen, Z. Chen, J. Janjic, V. Daeichin, Z.-Y. Chang, E. Noothout, G. van Soest, M. D. Verweij, N. de Jong, and M. A. P. Pertijs, "A front-end ASIC with high-voltage transmit switching and receive digitization for 3-D forward-looking intravascular ultrasound imaging," *IEEE Journal of Solid-State Circuits*, vol. 53, no. 8, pp. 2284–2297, 2018.

[7] G. Yun, K. Jeong, H. Choi, S. Nam, C. Oh, H. J. Lee, S. Ha, and M. Je, "A 2pA/$\sqrt{\text{Hz}}$ current-conveyor-assisted ultrasound receiver with 25pF CMUT parasitic capacitance," in *2023 IEEE Asian Solid-State Circuits Conference (A-SSCC)*, 2023, pp. 1–3.

[8] E. Kang, M. Tan, J.-S. An, Z.-Y. Chang, P. Vince, N. Sénégond, T. Mateo, C. Meynier, and M. Pertijs, "A 2pA/$\sqrt{\text{Hz}}$ transimpedance amplifier for miniature ultrasound probes with 36dB continuous-time gain compensation," in *2020 IEEE International Solid-State Circuits Conference - (ISSCC)*, 2020, pp. 354–356.

[9] P. Wang, C. Ma, C. Chen, Z. Hong, and J. Xu, "A 5.34 nV/$\sqrt{\text{Hz}}$, 65.9dB PSRR, 0.0068mm^2/channel LNA array for pitch-matched ultrasound receiver," in *2024 IEEE European Solid-State Electronics Research Conference (ESSERC)*, 2024, pp. 45–48.

[10] K. Chen, H.-S. Lee, and C. G. Sodini, "A column-row-parallel ASIC architecture for 3-D portable medical ultrasonic imaging," *IEEE Journal of Solid-State Circuits*, vol. 51, no. 3, pp. 738–751, 2016.

[11] H. Attarzadeh, Y. Xu, and T. Ytterdal, "A low-power high-dynamic-range receiver system for in-probe 3-D ultrasonic imaging," *IEEE Transactions on Biomedical Circuits and Systems*, vol. 11, no. 5, pp. 1053–1064, 2017.

[12] P. Guo, Z. Chang, E. Noothout, H. Vos, J. Bosch, N. de Jong, M. Verweij, and M. Pertijs, "A pitch-matched analog front-end with continuous time-gain compensation for high-density ultrasound transducer arrays," in *ESSCIRC 2021 - IEEE 47th European Solid State Circuits Conference (ESSCIRC)*, 2021, pp. 163–166.

[13] Y. Lu, Q. Wang, and D. A. Horsley, "Piezoelectric micromachined ultrasonic transducers with increased coupling coefficient via series transduction," in *2015 IEEE International Ultrasonics Symposium (IUS)*, 2015, pp. 1–4.

[14] A. Singhvi, A. Fitzpatrick, and A. Arbabian, "An electronically tunable multi-frequency air-coupled CMUT receiver array with sub-100μPa minimum detectable pressure achieving a 28kb/s wireless uplink across a water-air interface," in *2022 IEEE International Solid-State Circuits Conference (ISSCC)*, vol. 65, 2022, pp. 498–500.

[15] Y. Hopf, B. Ossenkoppele, M. Soozande, E. Noothout, Z.-Y. Chang, C. Chen, H. Vos, H. Bosch, M. Verweij, N. De Jong, and M. Pertijs, "A pitch-matched ASIC with integrated 65V TX and shared hybrid beamforming ADC for catheter-based high-frame-rate 3D ultrasound probes," in *2022 IEEE International Solid-State Circuits Conference (ISSCC)*, vol. 65, 2022, pp. 494–496.